Chinese Journal of
POLYMER SCIENCE

RESEARCH ARTICLE

https://doi.org/10.1007/s10118-026-3793-4
Chinese J. Polym. Sci.

Self-repairing and Durable Icephobic Coatings Based on Soluble Polydimethylsiloxane Covalent Adaptable Networks for Deicing

An-Ning Cen[a,†], Yin-Da Zhu[a,†], Ke Xu[b], De-Zhong Wen[a], Tong-Fei Wu[a,c*], Nuo Cao[b], and Xue-Lin Tian[a]

[a] *School of Materials Science and Engineering, Sun Yat-sen University, Guangzhou 510275, China*
[b] *State Key Laboratory of Environmental Adaptability for Industrial Products, China National Electric Apparatus Research Institute Co., Ltd., Guangzhou 510663, China*
[c] *Institute of Green Chemistry and Molecular Engineering, Sun Yat-sen University, Guangzhou 510275, China*

Electronic Supplementary Information

Abstract Passive anti-icing approaches utilizing icephobic surfaces present innovative solutions that require minimal energy, are simple to maintain, and are environmentally sustainable, garnering considerable interest. However, icephobic surfaces may encounter challenges related to environmental adaptability, which diminishes their durability. To mitigate this issue, we developed soluble polydimethylsiloxane covalent adaptable networks (PDMS CANs) for low-modulus icephobic coatings with intrinsic self-repairing capability. These soluble PDMS CANs were synthesized from diol-terminated PDMS, which underwent dynamic end-cross-linking through dioxaborolane linkages. The end-linked structure enabled dissolution in solvents such as ethyl acetate. Once the solvent was removed, the dynamic cross-linked networks re-formed. This feature made PDMS CANs suitable for processing methods such as solution casting or coating. The cross-linking density of the CANs could be modified by varying the chemical formulation. The effects of cross-linking density on mechanical properties, self-repairing capability, and icephobic performance were examined. To further enhance deicing performance, silicone oil was incorporated into the PDMS CANs as a lubricant. The relationship between icephobic performance and oil content was explored. The optimal ice adhesion strength, achieved at an oil content of 40 wt%, was approximately 7.1 kPa at −10 °C. The coatings demonstrated good durability throughout icing-deicing cycles. This study highlights the potential of self-repairing, low-modulus elastic coatings based on CANs for large-area deicing applications.

Keywords Covalent adaptable networks; Deicing; Low-modulus elastic coatings; Self-repairing; Lubricating

Citation: Cen, A. N.; Zhu, Y. D.; Xu, K.; Wen, D. Z.; Wu, T. F.; Cao, N.; Tian, X. L. Self-repairing and durable icephobic coatings based on soluble polydimethylsiloxane covalent adaptable networks for deicing. *Chinese J. Polym. Sci.* https://doi.org/10.1007/s10118-026-3793-4

INTRODUCTION

Icing is a prevalent natural occurrence that causes significant problems in infrastructure, transportation, power transmission systems, and renewable energy facilities.[1−3] To address the challenges posed by icing, various advanced anti-icing and de-icing technologies have been developed. These technologies are typically categorized into active and passive approaches, based on their operational principles and energy demands.[4] Active approaches work to prevent, melt, and eliminate ice by utilizing external energy or chemical agents, which provide rapid response times and high de-icing efficiency.[5] In contrast, passive approaches achieve inherent icephobic capabilities through modifications to material surfaces and the design of microstructures, such as superhydrophobic surfaces, slippery liquid-infused porous surfaces (SLIPS), and low-modulus elastic coatings.[6,7] They present innovative solutions that consume minimal energy, are easy to maintain, are environmentally friendly, and have attracted significant interest.[8]

Low-modulus elastic coatings take advantage of the mechanical modulus mismatch with the ice layer (approximately 8.5 GPa)[2]. This discrepancy promotes interfacial cavitation and fracture under applied stress, thereby aiding the detachment of ice. Several hydrophobic elastic polymers, including polydimethylsiloxane (PDMS), polyurethane (PU), and fluoroelastomer, have been assessed as low-modulus elastic coatings characterized by low modulus (typically<1 MPa) and low surface energy.[9,10] These materials demonstrate considerable potential for achieving remarkably low ice-adhesion strength (<10 MPa). Furthermore, it was discovered that the force required to detach ice becomes nonproportional to the size of the ice once it exceeds a critical threshold, referred to as the critical ice-bonded length.[2] In such cases, the uneven distribution of interfacial stress between the ice and substrate is thought to play a crucial role in altering the interfacial failure modes, facilitating rapid crack propagation along the interface under minimal external forces, resulting in an ultralow ice adhesion strength (*e.g.*, about 4 kPa).[11] This size-

* Corresponding author, E-mail: wutongfei@mail.sysu.edu.cn
† These authors contributed equally to this work.
Received May 28, 2026; Accepted June 22, 2026; Published online September 4, 2026

dependent behavior permits low-modulus elastic coatings to facilitate the easy removal of large ice formations. Despite their many advantages, low-modulus elastic coatings may face challenges in terms of performance stability and durability, similar to other soft passive anti-icing and de-icing surfaces. Mechanical damage, such as scratches and impacts, inevitably roughens the surface, creating microscopic or macroscopic concave-convex patterns. Ice can become embedded in these surface defects, leading to mechanical interlocking and increased ice adhesion strength, which limits the de-icing efficiency.

Inspired by the natural ability of organisms to heal after sustaining injuries, the integration of self-repairing attributes into anti-icing/deicing coatings has been proposed as an effective strategy to enhance performance reliability and prolong the lifespan.[12–14] The mechanisms of repair can be generally divided into two categories: extrinsic and intrinsic.[15] Extrinsic mechanisms rely on the release of healing agents that are pre-embedded within the matrix, whereas intrinsic mechanisms operate through reversible cleavage and reformation of dynamic bonds.[12,16] This latter mechanism allows for repetitive repair. Polymer networks crosslinked with dynamic covalent bonds, referred to as covalent adaptive networks (CANs), can reorganize their structure through topological rearrangement, thereby exhibiting intrinsic self-repair and thermally activated reprocessing capabilities. Commonly studied dynamic covalent bonds include disulfide bonds, transesterification linkages, imine bonds, and dioxaborolane linkages.[17] In recent decades, there has been increasing interest in the chemistry of self-repair, with significant advancements highlighted in recent reviews.[18,19]

In this study, we took advantage of PDMS CANs to demonstrate the potential of self-repairing low-modulus elastic coatings for large-scale de-icing applications. PDMS CANs were prepared from diol-terminated PDMS, which was dynamically end-crosslinked *via* dioxaborolane linkage. The bond-exchange reaction of dioxaborolanes can occur without the aid of a catalyst at relatively low temperatures, such as room temperature, which will facilitate the autonomous self-repair of CANs during de-icing operations.[20–22] It was also found that the as-prepared PDMS CANs were also found to be soluble in ethyl acetate, which aided the molding process. The crosslinking density was tuned by varying the molecular weight of the diol-terminated PDMS and the molar ratio of the boronic acid group to the diol group, and their effects on the mechanical properties, self-repairing behavior, and icephobic properties were investigated. To further enhance the de-icing performance, the PDMS CANs were infused with a silicone oil lubricant. The correlation between the icephobic properties and oil content has also been explored for sustainable applications.

EXPERIMENTAL

Materials

Octamethylcyclotetrasiloxane (D4, >98.0%), tetramethylammonium hydroxide pentahydrate (TMAH, ≥97%), 1,4-benzenediboronic acid (BDA, ≥95%), 1,4-benzenediboronic acid bis(pinacol) ester (≥95%) and methanol (≥99.8%) were acquired from Shanghai Aladdin Biochemical Technology Co., Ltd. 1,3-Bis(3-aminopropyl) tetramethyldisiloxane (BAPTS, 97%), glycidol (GLY, 97%), and ethyl acetate (≥99.7%) were purchased from Shanghai Macklin Biochemical Technology Co., Ltd. Trimethylsiloxy-terminated polydimethylsiloxane oil (*t*-PDMS, M_n≈770 g/mol) was obtained from Alfa Aesar (Thermo Fisher Scientific, Inc.). All chemicals were used as received, without any additional purification.

Synthesis of 1,2-Diol-terminated Polydimethylsiloxane

The synthesis of 1,2-diol-terminated polydimethylsiloxane (diol-PDMS-diol) was performed in a two-step process, as illustrated in Fig. 1. The initial step involved the preparation of aminopropyl-terminated polydimethylsiloxane (NH_2-PDMS-NH_2) *via* ring-opening polymerization of D4, employing BAPTS as an end-capping agent and TMAH as the catalyst.[23] In a typical procedure, specific quantities of D4 and TMAH (pre-dissolved in 1mL of methanol) were charged into a round-bottom flask in accordance with the stoichiometric ratios provided in Table S1 (in the electronic supplementary information, ESI). The mixture was subjected to stirring and heated to 60 °C under reduced pressure (<10 kPa) for 1 h to remove the methanol. Subsequently, the temperature was raised to 80 °C, and the reaction mixture was stirred overnight after the dropwise addition of BAPTS.

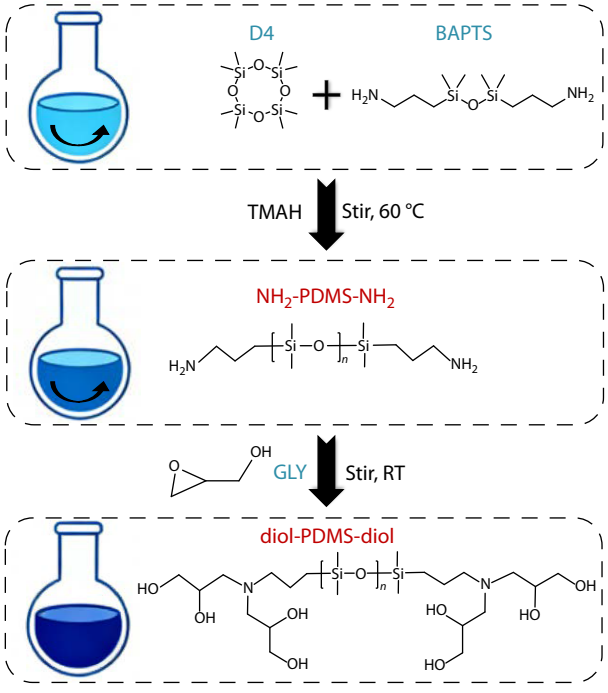

Fig. 1 The process of preparing 1,2-diol-terminated PDMS (diol-PDMS-diol).

Following that, the temperature was further elevated to 140 °C, leading to the thermal decomposition of the catalyst TMAH. The intermediate NH_2-PDMS-NH_2 was acquired after the removal of the decomposition products under reduced pressure at 150 °C. In the second phase, an appropriate amount of GLY was added to the as-prepared NH_2-PDMS-NH_2 along with a mixed solvent of ethyl acetate and methanol (5/1, *V*/*V*). The solvent-to-NH_2-PDMS-NH_2 volume ratio was

approximately 1/1. The epoxide ring-opening reaction proceeded with continuous stirring at room temperature for 8 h. Thereafter, the solvent was removed under reduced pressure at 60 °C, yield the diol-PDMS-diol. The weight-average molecular weights (M_w) of the three diol-PDMS-diol samples prepared were determined to be 10.4, 14.3 and 21.3 kg/mol through gel permeation chromatography (Fig. S1 in ESI), as summarized in Table S2 (in ESI).

Preparation of PDMS CANs Based on Dioxaborolane

PDMS CANs with varying levels of cross-linking were prepared from diol-PDMS-diol and BDA, as shown in Fig. 2(a). The formulation details are presented in Table 1, where the BA/diol ratio denotes the molar ratio of the boronic acid group to 1,2-diol group. Specific amounts of diol-PDMS-diol and BDA were dissolved separately in a mixed solvent composed of ethyl acetate and methanol (5/1, *V*/*V*) at concentration of 0.5 g/mL. The BDA solution was then introduced into the diol-PDMS-diol solution while stirring. The resulting mixture was then maintained at room temperature for 6 h. PDMS CANs were obtained by evaporation of the solvent under reduced pressure at 60 °C. To facilitate molding, precursor solutions, including diol-PDMS-diol and BDA, were prepared by redissolving the PDMS-CAN samples in ethyl acetate at a concentration of 0.5 g/mL. The final PDMS-CAN samples were produced by evaporating the solvent under ambient conditions.

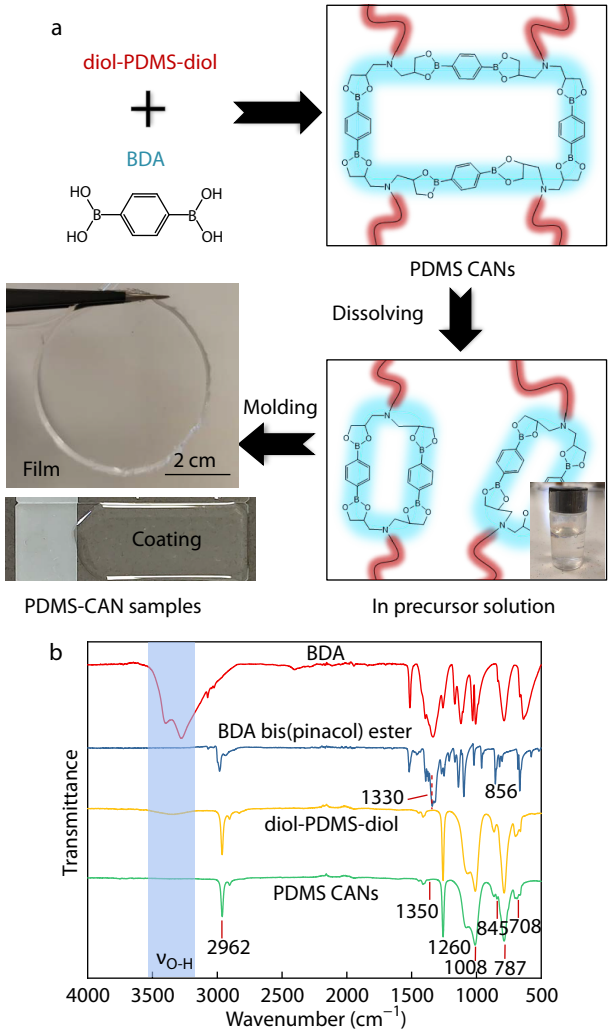

Fig. 2 (a) Schematic pathway to the preparation of PDMS CANs from diol-PDMS-diol and BDA; (b) FTIR spectra of PDMS CANs, diol-PDMS-diol, BDA and its bis(pinacol) ester.

Table 1 Formulation for preparation of PDMS CANs.

Sample	diol-PDMS-diol content (g)	BDA content (mg)	BA/diol ratio
PDMS-CAN1	5.0 (10.4) [a]	132	0.8
PDMS-CAN2	5.0 (14.3)	88	0.8
PDMS-CAN3	5.0 (21.3)	66	0.8
PDMS-CAN4	5.0 (14.3)	66	0.6
PDMS-CAN5	5.0 (14.3)	77	0.7
PDMS-CAN6	5.0 (14.3)	99	0.9
PDMS-CAN7	5.0 (14.3)	111	1.0

[a] The figure enclosed in parentheses represents M_w, with the unit being kg/mol.

Preparation of Oil-infused PDMS CANs

For the lubricant-infused samples, a designated amount of *t*-PDMS oil was incorporated into the precursor solution. Oil-infused PDMS-CAN samples were produced by solvent evaporation under ambient conditions.

Characterizations

The average molecular weight and polydispersity index of PDMS were determined *via* gel permeation chromatography using a 1260 Infinity II HPLC GPC/SEC System (Agilent Technologies), with polystyrene serving as the calibration standard. The measurements were conducted at a temperature of 40 °C, employing tetrahydrofuran as the eluent at a flow rate of 1.00 mL/min. Fourier transform infrared spectra (FTIR) were acquired using a Nicolet iS10 spectrometer (Thermo Fisher Scientific) in the attenuated total reflectance (ATR) mode. All the spectra were recorded from 4000 cm^{-1} to 500 cm^{-1} with a resolution of 2 cm^{-1}. Surface morphology was investigated using a DMD2700 M optical microscope (Leica Camera AG). The tensile properties of the samples were assessed using a HZ-1007C universal testing machine (Lixian Instrument Technology) at ambient temperature. The gauge length was maintained at 20 mm, and the crosshead speed was set to 100 mm/min. Five specimens were evaluated for each specimen. The elongation at break was defined as the ratio of the extension length at the fracture point to the original gauge length of the specimen. The tensile strength was determined by dividing the maximum force exerted during the tensile test by the initial cross-sectional area of the sample. The Young's moduli were calculated using the slopes of the tensile stress-strain curves within a strain range of 1%–5%. The shear stress relaxation behavior of the samples was investigated using an MCR 302 rheometer (Anton Paar GmbH) at different temperatures. Prior to the relaxation test, the specimens were heated to the desired temperature and maintained for 15 min to attain thermal equilibrium. During the test, a constant strain of 3% and axial force of about 1 N were applied. Surface wettability was assessed by measuring the static water contact angle with the aid of a DSA100S drop shape analyzer (KRÜSS Scientific). To guarantee precision and reproducibility, three separate measurements were performed with droplets of 5 μL at different locations on each specimen. The ice adhesion strength (σ_{ice}) was measured at –10 °C *via* the horizontal shear method: $\sigma_{ice} = F/A$, where F is the peak value of shear force to

https://doi.org/10.1007/s10118-026-3793-4

push ice columns at a velocity of 0.05 mm/s and A is the ice contact area.[2] For the repeated tests, the data were checked *via* one-way ANOVA, and multiple comparisons were conducted using Tukey's post hoc test. The threshold for statistical significance was $p < 0.05$.

RESULTS AND DISCUSSION

Characterization of PDMS CANs Based on Dioxaborolane

PDMS CANs were prepared through a condensation reaction involving diol-PDMS-diol and BDA, as shown in Fig. 2(a). Diol-PDMS-diol loses its fluidity after cross-linking with BDA. The resulting PDMS-CAN samples were soluble in ethyl acetate, which could be attributed to their end-linked architecture. It has been proposed that their cross-linked structures could be transformed into soluble linear forms through topological rearrangements with the aid of solvation. Upon removal of the solvent, the crosslinked structures were restored. By utilizing the precursor solutions, PDMS CANs can be readily shaped into films and coatings using the solution casting or coating method, particularly for large-area applications. The chemical structures of the PDMS CANs were characterized by Fourier transform infrared spectroscopy (FTIR) and compared with diol-PDMS-diol, BDA, and its bis(pinacol) ester. As shown in Fig. 2(b), the FTIR spectrum of PDMS CANs revealed characteristic absorption bands associated with the Si—CH_3 groups: 708 cm^{-1} (Si—C symmetric stretching), 787 cm^{-1} (C—H asymmetric wagging and Si—C asymmetric stretching), 862 cm^{-1} (C—H symmetric rocking), 1260 cm^{-1} (C—H symmetric bending), 1409 cm^{-1} (C—H asymmetric bending), 2906 cm^{-1} (C–H symmetric stretching), and 2962 cm^{-1} (C—H asymmetric stretching).[24] The significant band at 1008 cm^{-1} corresponds to the stretching vibration of the Si—O—Si backbone.[25] In contrast to diol-PDMS-diol, the absence of O—H absorption (3400 cm^{-1}) in PDMS CANs indicates the consumption of OH groups by the condensation reaction to form dioxaborolanes. The absorption bands around 1330 and 856 cm^{-1} are attributed to dioxaborolane and aromatic rings, respectively, in the bis(pinacol) ester of BDA.[26] They were also recorded in the PDMS CANs.

The de-icing mechanism based on low-modulus icephobic materials relies on the difference in the modulus between the material and ice layer. The influence of the molecular weight (M_w) of diol-PDMS-diol on the mechanical properties of the PDMS CANs was assessed through uniaxial tensile testing. The results for the corresponding Young's modulus, tensile strength, and elongation at break are summarized in Fig. 3. The Young's modulus of the PDMS CANs decreased as the M_w of diol-PDMS-diol increased. As illustrated in Fig. 3(A), the Young's modulus decreased from 0.22 MPa to 0.15 MPa as M_w increasing from 10.4 kg/mol to 21.3 kg/mol. The molar ratio of the boronic acid group to the 1,2-diol group ($R_{BA/diol}$, BA/diol ratio) also influenced the mechanical properties of PDMS CANs. In Fig. 3(B), the Young's modulus rises from 0.04 MPa to 0.78 MPa as the BA/diol ratio increases from 0.7 to 1.0 for PDMS-CAN samples with M_w = 14.3 kg/mol. This behavior can be attributed to the positive correlation between the modulus and cross-linking density:[27] as the M_w of diol-PDMS-diol decreases or the BA/diol ratio increases, the cross-linking density in PDMS CANs increases, resulting in an increase in Young's modulus.

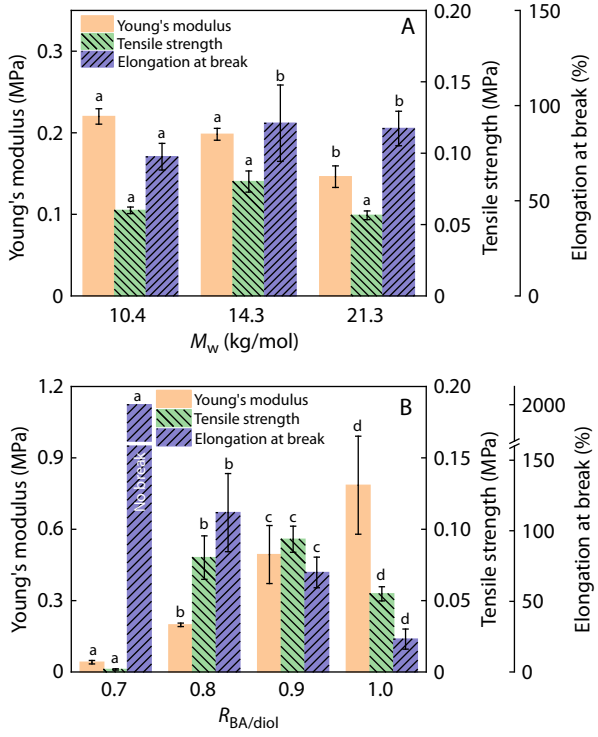

Fig. 3 Tensile properties of PDMS-CAN samples with different (A) M_w of diol-PDMS-diol and (B) BA/diol ratios. The error bars represent the standard deviation, and different letters indicate significant differences.

PDMS CANs were coated onto glass substrates from the precursor solutions to investigate their icephobic properties. The wettability was first studied by measuring the water contact angle.[28] The water contact angles of all PDMS-CAN coatings were stable at approximately 120° (see Fig. S2 in ESI), which is essentially equivalent to the intrinsic value of PDMS materials reflecting a high degree of hydrophobicity.[29] Icephobic properties are typically evaluated by measuring the ice-adhesion strength. Fig. 4 presents the ice adhesion strengths of PDMS-CAN coatings made from diol-PDMS-diol with different M_w at −10 °C. It can be seen from Fig. 4(A) that the ice adhesion strengths were determined to be 165.6, 90.1, and 61.3 kPa, for the coatings with M_w=10.4, 14.3 and 21.3 kg/mol, respectively, suggesting a declining trend of ice adhesion strength with increasing the M_w of diol-PDMS-diol. It was found that the BA/diol ratio also had an impact on the ice-adhesion strength of the PDMS-CAN coatings. It can be seen from Fig. 4(B) that the ice adhesion strengths exhibited an increasing trend with increasing the BA/diol ratio, from 64.5 kPa for BA/diol ratio = 0.7 to 91.8 kPa for BA/diol ratio = 1.0. Considering the mechanical properties of PDMS CANs, a higher Young's modulus corresponds to a higher ice adhesion strength.

Beyond the modulus of the coatings, the coating thickness also constitutes a critical factor influencing the ice-adhesion strength. For a coating with a planar surface and uniform composition, the relationship among the ice adhesion strength (σ_{ice}), modulus (E), thickness (h), and adhesion work

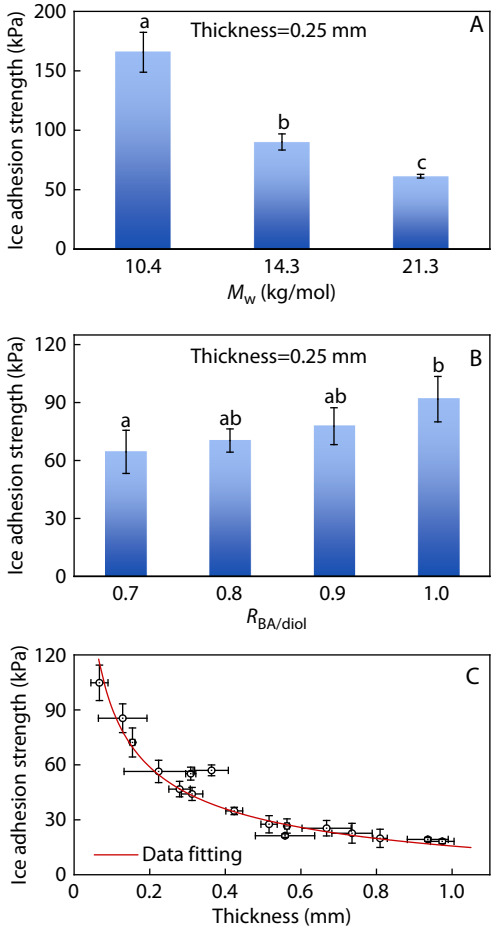

Fig. 4 Ice adhesion strength of PDMS-CAN coatings with different (A) M_w of diol-PDMS-diol and (B) BA/diol ratios. (C) Ice adhesion strength as a function of thickness for the PDMS-CAN coating (M_w = 14.3 kg/mol and BA/diol ratio = 0.8). The error bars represent the standard deviation, and different letters indicate significant differences.

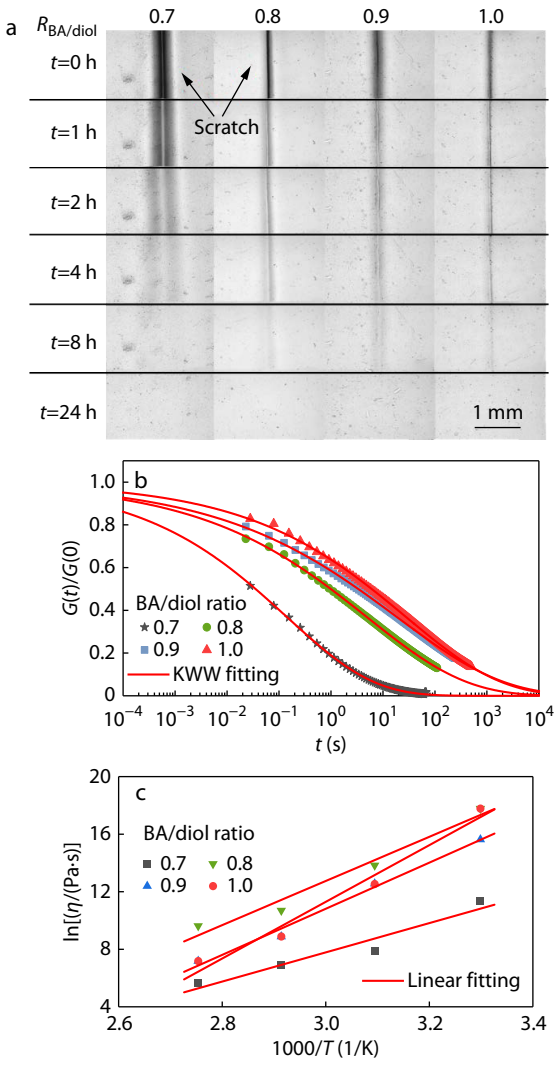

Fig. 5 (a) Photographs to demonstrate the scratch-repairing behavior of PDMS-CAN coatings; (b) The normalized stress-relaxation curves, $G(t)/G(0)$, of PDMS-CAN samples with different BA/diol ratios at 30°C and (b) Plots of lnη as a function of 1000/T. The M_w of diol-PDMS-diol utilized in the preparation of PDMS CANs was 14.3 kg/mol. The sub-millimetre scratches created with a surgical blade with a depth of 0.25mm and no control over width.

(W_a) can be described by the following relationship:[2] $\sigma_{ice} \propto \sqrt{EW_a/h}$. Fig. 4(C) depicts the ice-adhesion strength of the PDMS-CAN coating as a function of thickness. The ice-adhesion strength exhibited a steep initial decline with increasing thickness, which subsequently plateaued at greater thicknesses. The above equation was used to fit the data with adhesion work as an undetermined coefficient, indicating satisfactory agreement between the experimental data and the empirical relationship. When the coating thickness approaches 1.0 mm, the ice adhesion strength was reduced to 19.3 kPa.

The dynamic properties of the PDMS CANs were examined by analyzing their self-repair behavior. The exceptional flexibility of PDMS, having a glass transition temperature (T_g) of about −120 °C, would benefit the mobility of strands for the topological rearrangement of PDMS CANs.[30] Fig. 5(a) illustrates the scratch-healing process of PDMS-CAN coatings with varying BA/diol ratios at ambient temperature (23 °C). It is evident that all PDMS CANs were capable of nearly repairing a sub-millimeter scratch within 8 h, with complete repair achieved within 24 h. In addition, the dynamic properties of the PDMS CANs were further investigated through stress relaxation measurements conducted at various temperatures. It was found that the relaxation modulus curves could be described by the Kohlrausch-Williams-Watts (KWW) equation[31]

$$G(t) = G(0)\exp[-\left(\frac{t}{\tau_{KWW}}\right)^{\beta}] \quad (1)$$

where $G(t)$ is the relaxation modulus, $G(0)$ is the initial relaxation modulus, τ_{KWW} is the characteristic relaxation time, and β represents the stretched exponent, which is typically located in the range of $0 < \beta \leq 1$. Fig. 5(b) shows the normalized relaxation modulus curves for PDMS CANs with varying BA/diol ratios at a temperature of 30 °C.

Zero-shear viscosity (η) is given by $\int_0^\infty G(t)dt$, which equals $\Gamma(1/\beta)\tau_{KWW}/\beta$, where Γ is the gamma function.[32] To quantitatively evaluate the energy barrier for topological rearrange-

ment within the PDMS CANs, the apparent activation energy (E_a) was derived from η using the Arrhenius equation[33]

$$\ln\eta = \ln\eta_0 + E_a/RT \quad (2)$$

where R is the gas constant (8.314 J/(mol·K)), and η_0 is the pre-exponential factor. The plots of $\ln\eta$ against $1/T$ are shown in Fig. 5(c). The values of E_a values were determined to be 84.5, 128, 133, and 164 kJ/mol, for BA/diol ratios of 0.7, 0.8, 0.9, and 1.0, respectively. This indicates that an increase in the BA/diol ratio in the PDMS CANs led to a heightened energy barrier for network rearrangement. In the context of boronic ester-based CANs, topological rearrangement is driven by two competing associative exchange reactions: the exchange of dioxaborolanes with 1,2-diol and the metathesis reaction involving dioxaborolanes. The value of E_a for the former reaction was reported to be 15 kJ/mol,[34] whereas the E_a for the latter reaction was close to 50 kJ/mol.[21] A low E_a permits bond exchange at relatively low temperatures. For PDMS CANs, an increase in the BA/diol ratio enhances the contribution from the metathesis pathway. Furthermore, it is well established that the E_a of topological rearrangement derived from η in CANs is also associated with segmental motion, which may differ significantly from the intrinsic characteristics of the bond exchange reaction.[35] For a specific polymer, a greater cross-linking density of CANs is generally associated with a higher value of E_a.[36]

Characterization and Icephobic Properties of Oil-infused PDMS CANs

Lubricants are expected to improve the efficacy of icephobic coatings because they have the potential to diminish the coating modulus and weaken the cohesive forces at the interface. Low-molecular-weight PDMS oil was incorporated into the PDMS CANs to serve as a lubricant for the creation of oil-infused PDMS CANs. The impact of the oil content on the mechanical properties of the PDMS-CAN samples was evaluated using uniaxial tensile testing. The results regarding the Young's modulus, tensile strength, and elongation at break are shown in Fig. 6(A). It is evident that the Young's modulus exhibited a decreasing trend from 0.20 MPa to 0.05 MPa as the oil content increases from 0 wt% to 40 wt%. Fig. 6(B) shows the mechanical self-repairing capability of the oil-infused PDMS-CAN sample with an oil content of 10 wt% over the course of 1 h at ambient temperature. To quantitatively assess the mechanical healing efficiency, the tensile properties of the oil-infused PDMS-CAN samples were compared before and after the repair process. Fig. 6(C) presents the tensile test outcomes for various healing durations. After one hour of healing, the oil-infused PDMS-CAN sample regained 80%−90% of its initial tensile strength and Young's modulus. Following two hours of healing, both the tensile strength and Young's modulus were restored to levels comparable to those in the pristine state.

Fig. 7(a) depicts the scratch repair process in oil-infused PDMS-CAN coatings at ambient temperature. The oil-infused PDMS CANs achieved complete repair within 4 h, demonstrating a faster repair rate than pristine PDMS CANs. This observation indicates that the presence of small oil molecules enhances the segmental mobility, facilitating the topological rearrangement of networks. It should also be noted that these small molecules may increase the distance between network junctions, consequently decreasing the bond-exchange rate. The ultimate outcome was determined by the balance between these two effects. The water contact angles of the oil-infused PDMS-CAN coatings are shown in Fig. 7(b). These angles remained consistently around 120°, identical to those of the oil-free samples, indicating a relatively high degree of hy-

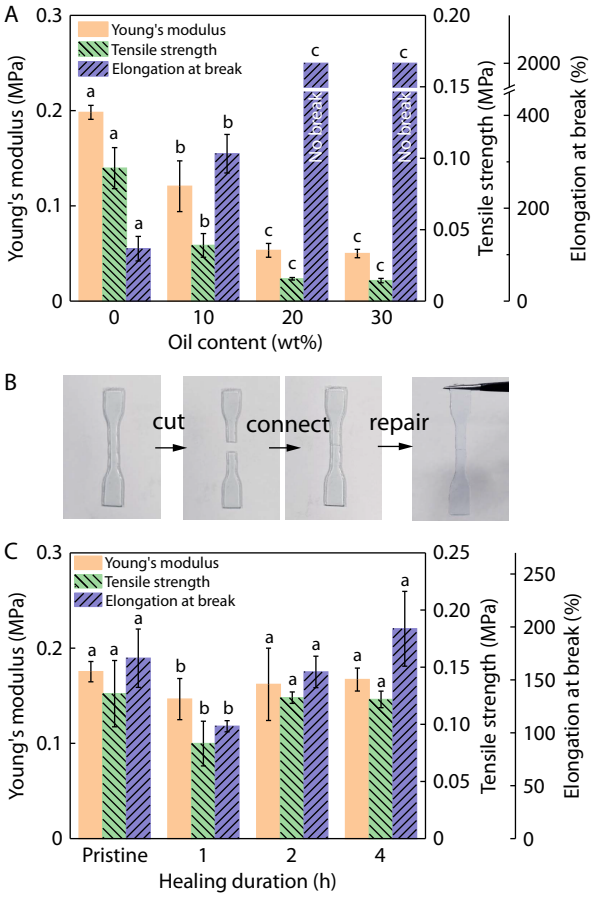

Fig. 6 (A) Tensile properties of oil-infused PDMS-CAN samples with different oil contents (M_w=14.3 kg/mol and BA/diol ratio = 0.8); (B) Photographs demonstrating the mechanical self-repairing ability of oil-infused PDMS CANs; (C) The tensile properties of the oil-infused PDMS-CAN sample after various healing durations. The error bars represent the standard deviation, and different letters indicate significant differences.

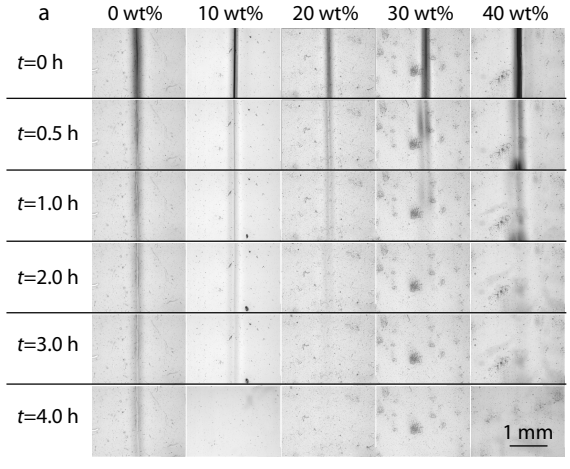

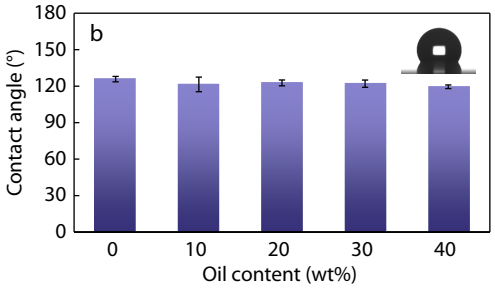

Fig. 7 (a) Photographs to demonstrate the scratch-repairing behavior of oil-infused PDMS-CAN coatings; (b) Water contact angles of oil-infused PDMS-CAN coatings with different oil contents. The inset is a photograph of a sessile droplet on the coating surface for the measurement of contact angles. The error bar represents standard deviation, different letters indicate significant differences. The sub-millimetre scratches created with a surgical blade with a depth of 0.35 mm and no control over width.

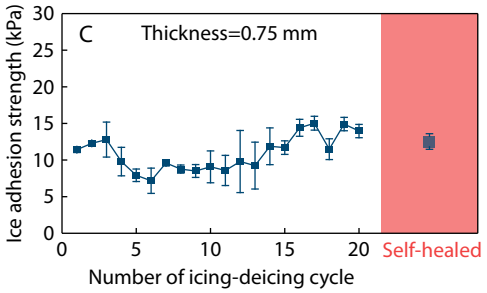

Fig. 8 (A) Ice adhesion strength of oil-infused PDMS-CAN coatings with different oil content; (B) Ice adhesion strength of the sample with an oil content of 20 wt% at different thickness. (C) Ice adhesion strength during icing-deicing cycles and after scratch-repairing for the sample with an oil content of 40 wt% . The error bar represents standard deviation, different letters indicate significant differences.

drophobicity.

The effect of the oil content on the ice-adhesion strength of oil-infused PDMS-CAN coatings is shown in Fig. 8(A). It can be seen that the ice adhesion strength displayed a consistent decreasing trend as the oil content increased from 0 wt% to 40 wt%, ultimately reaching a low value of 11.5 kPa. The effect of the coating thickness on the ice-adhesion strength was also evaluated for oil-infused PDMS-CAN coatings. As illustrated in Fig. 8(B), when the thickness increased from 0.24 mm to 1.44 mm, the ice adhesion strength of the coating with 20 wt% oil content significantly decreased from 77.9 kPa to 11.5 kPa, following an inverse relationship with the square root of thickness. The durability of the oil-infused PDMS-CAN coatings was assessed through icing–de-icing cycles. Fig. 8(C) shows that there was no notable reduction in the ice-adhesion strength of the coating with 40 wt% oil content, which maintained a stable ice adhesion strength within the range of 7−15 kPa throughout the testing period. After 20 cycles of icing and de-icing, the ice-adhesion strength remained steady at approximately 13 kPa, demonstrating that the oil-infused PDMS-CAN coatings possessed reliable icephobic properties. The oil was supposed to serve as a sacrificial medium at the interface between the coating and ice layer, as in the SLIPS. No notable changes in the weight of the coatings were observed after 20 cycles. Extended testing is necessary to gather additional data. It is important to note that the ice adhesion strength of the scratch-repaired sample exhibited minimal change compared to the undamaged sample (highlighted in red in Fig. 8C), suggesting that oil-infused PDMS-CAN coatings can restore their icephobic properties following physical damage, thereby enhancing their durability.

Weak ice adhesion can facilitate the formation of cavitations and fractures at the interface between ice and low-mod-

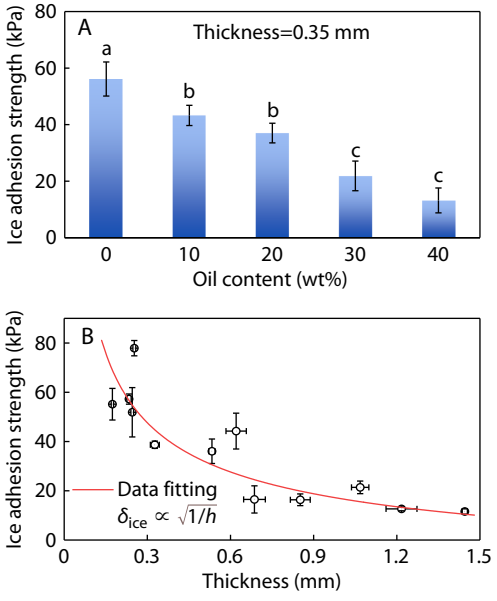

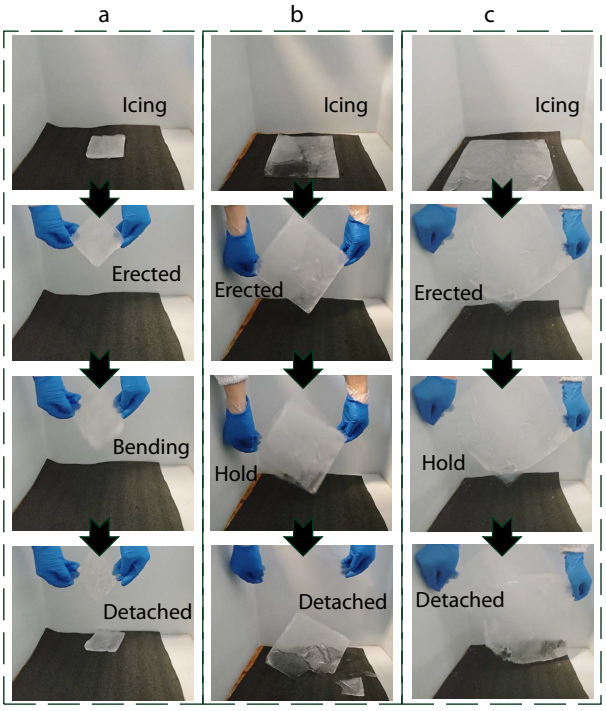

Fig. 9 Demonstration of oil-infused PDMS-CAN coatings utilized for deicing, showcasing various icing areas of (a) 10 cm × 10 cm, (b) 20 cm × 20 cm, and (c) 30 cm × 30 cm.

https://doi.org/10.1007/s10118-026-3793-4

ulus elastic coatings when a shear force is applied, resulting in ice detachment. To demonstrate the effectiveness of oil-infused PDMS-CAN coatings in de-icing applications, a series of de-icing experiments was performed, focusing on substantial ice accumulation. Acrylic glass sheets with dimensions—10 cm × 10 cm, 20 cm × 20 cm, and 30 cm × 30 cm—were uniformly coated with a formulation containing 40 wt% oil, achieving a nominal thickness of approximately 0.75 mm. These coated sheets were positioned horizontally within a cold chamber maintained at −10 °C and the thickness of the surface ice increased as icing progressed. When the thickness of the surface ice reached approximately 10.0 mm, the sheets were raised vertically to facilitate observation of ice detachment. As depicted in Fig. 9, in the case of a 10 cm × 10 cm ice layer, its own gravity was insufficient for ice detachment, requiring minor bending to promote interfacial cavitation and final detachment. In contrast, for larger ice layers (20 cm × 20 cm and 30 cm × 30 cm), the gravitational forces were sufficient to induce interfacial cavitation and fractures, leading to spontaneous detachment of the ice layers. These experimental results validate that oil-infused PDMS CANs have significant potential for passive anti-icing approaches.

CONCLUSIONS

In summary, soluble PDMS CANs were developed from diol-terminated PDMS that underwent dynamic end-cross-linking *via* dioxaborolane linkages. Their end-linked structure allows them to dissolve in solvents such as ethyl acetate. Upon removal of the solvent, the dynamic cross-linked networks were reestablished. This characteristic renders PDMS CANs appropriate for processing techniques, such as solution casting or coating. The mechanical properties of the PDMS CANs were tuned by adjusting the M_w of the diol-terminated PDMs and the BA/diol ratio. The Young's modulus of the PDMS CANs decreased as the M_w of the diol-terminated PDMS increased, whereas it increased with a higher BA/diol ratio owing to the increased cross-linking density. The ice adhesion strength of the PDMS CANs exhibited a positive correlation with Young's modulus and an inverse relationship with the square root of the coating thickness. By methodically adjusting the modulus and thickness, the ice-adhesion strength was minimized to a value of 19.3 kPa for PDMS CANs. The ice-adhesion strength decreased with an increase in the oil content. With the incorporation of 40 wt% oil, a notably low ice adhesion strength of 7.1 kPa was recorded at −10 °C, demonstrating excellent durability throughout icing and deicing cycles. Owing to the low ice-adhesion strength, the ice layer could be easily removed from oil-infused PDMS-CAN coatings *via* gravity. This study highlights the potential of self-repairing low-modulus elastic coatings based on icephobic CANs for large-scale deicing applications.

Conflict of Interests

The authors declare no interest conflict.

Electronic Supplementary Information

Electronic supplementary information (ESI) is available free of charge in the online version of this article at http://doi.org/10.1007/s10118-026-3793-4.

Data Availability Statement

The data supporting the findings of this study are available from the corresponding author upon reasonable request.

ACKNOWLEDGMENTS

This work was financially supported by the Guangdong Basic and Applied Basic Research Foundation (No. 2023A1515012899).

REFERENCES

1 Wang, Y.; Liao, Z.; Zeng, Q.; Li, G.; He, Y.; Yang, Y.; Song, Y.; Wang, L.; Liu, S.; Xuan, S.; Wang, X.; Ge, Y.; Yin, K. Robust and energy-effective electrothermal superhydrophobic film with micro-hexagonal groove array structure for anti/deicing. *Adv. Funct. Mater.* **2026**, *36*, e14771.
2 Golovin, K.; Dhyani, A.; Thouless, M. D.; Tuteja, A. Low–interfacial toughness materials for effective large-scale deicing. *Science* **2019**, *364*, 371–375.
3 Zhao, Y.; Guo, Q.; Lin, T.; Cheng, P. A review of recent literature on icing phenomena: Transport mechanisms, their modulations and controls. *Int. J. Heat Mass Transfer* **2020**, *159*, 120074.
4 Rekuviene, R.; Saeidiharzand, S.; Mažeika, L.; Samaitis, V.; Jankauskas, A.; Sadaghiani, A. K.; Gharib, G.; Muganlı, Z.; Koşar, A. A review on passive and active anti-icing and de-icing technologies. *Appl. Therm. Eng.* **2024**, *250*, 123474.
5 Shi, J.; Ke, S.; Wang, F.; Wang, W.; Wang, C. Recent advances in photothermal anti-/de-icing materials. *Chem. Eng. J.* **2024**, *481*, 148265.
6 Wang, T.; Zheng, Y.; Raji, A.-R. O.; Li, Y.; Sikkema, W. K. A.; Tour, J. M. Passive anti-icing and active deicing films. *ACS Appl. Mater. Interfaces* **2016**, *8*, 14169–14173.
7 Golovin, K.; Tuteja, A. A predictive framework for the design and fabrication of icephobic polymers. *Sci. Adv.* **2017**, *3*, e1701617.
8 Liu, Y.; Wu, Y.; Liu, S.; Zhou, F. Material strategies for ice accretion prevention and easy removal. *ACS Mater. Lett.* **2022**, *4*, 246–262.
9 Beemer, D. L.; Wang, W.; Kota, A. K. Durable gels with ultra-low adhesion to ice. *J. Mater. Chem. A* **2016**, *4*, 18253–18258.
10 Qi, H.; Lei, X.; Gu, J.; Zhang, Y.; Gu, X.; Zhao, G.; Yu, J. Low modulus of polydimethylsiloxane organogel coatings induced low ice adhesion. *Prog. Org. Coat.* **2023**, *177*, 107435.
11 Azimi Dijvejin, Z.; Jain, M. C.; Kozak, R.; Zarifi, M. H.; Golovin, K. Smart low interfacial toughness coatings for on-demand de-icing without melting. *Nat. Commun.* **2022**, *13*, 5119.
12 Li, B.; Cao, P.; Saito, T.; Sokolov, A. P. Intrinsically self-healing polymers: From mechanistic insight to current challenges. *Chem. Rev.* **2023**, *123*, 701–735.
13 Zhuo, Y.; Håkonsen, V.; He, Z.; Xiao, S.; He, J.; Zhang, Z. Enhancing the mechanical durability of icephobic surfaces by introducing autonomous self-healing function. *ACS Appl. Mater. Interfaces* **2018**, *10*, 11972–11978.
14 Zhao, X.; Peng, J.; Gao, S.; Zhu, K.; Zhao, Y.; Li, X.; Yuan, X. Self-healing anti-icing coatings prepared from PDMS polyurea. *Sci. China Technol. Sci.* **2021**, *64*, 1535–1543.
15 Hia, I. L.; Vahedi, V.; Pasbakhsh, P. Self-healing polymer composites: Prospects, challenges, and applications. *Polym. Rev.* **2016**, *56*, 225–261.
16 Wang, S.; Urban, M. W. Self-healing polymers. *Nat. Rev. Mater.* **2020**, *5*, 562–583.

Graphical Abstract

Self-repairing and Durable Icephobic Coatings Based on Soluble Polydimethylsiloxane Covalent Adaptable Networks for Deicing

An-Ning Cen, Yin-Da Zhu, Ke Xu, De-Zhong Wen, Tong-Fei Wu, Nuo Cao, and Xue-Lin Tian

Sun Yat-sen University; China National Electric Apparatus Research Institute Co., Ltd.

Self-repairing low-modulus icephobic covalent adaptable networks (CANs) are developed for large-scale deicing applications. The low ice adhesion strength is achieved by varying the molecular weight of polydimethylsiloxane (PDMS) precursor, cross-linker amount and oil content.

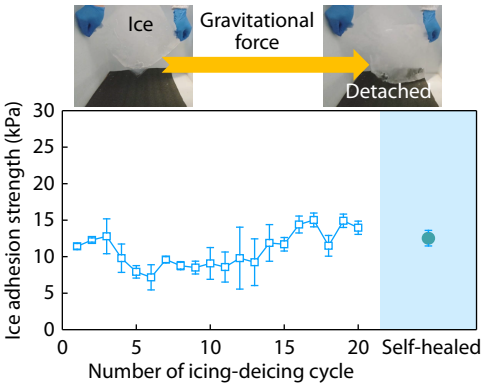

Chinese J. Polym. Sci. 2026 *https://doi.org/10.1007/s10118-026-3793-4*

17 Maes, S.; Badi, N.; Winne, J. M.; Du Prez, F. E. Taking dynamic covalent chemistry out of the lab and into reprocessable industrial thermosets. *Nat. Rev. Chem.* **2025**, *9*, 144–158.
18 Li, Z.; Yu, R.; Guo, B. Shape-memory and self-healing polymers based on dynamic covalent bonds and dynamic noncovalent interactions: synthesis, mechanism, and application. *ACS Appl. Bio Mater.* **2021**, *4*, 5926–5943.
19 Winne, J. M.; Leibler, L.; Du Prez, F. E. Dynamic covalent chemistry in polymer networks: a mechanistic perspective. *Polym. Chem.* **2019**, *10*, 6091–6108.
20 Marco-Dufort, B.; Iten, R.; Tibbitt, M. W. Linking molecular behavior to macroscopic properties in ideal dynamic covalent networks. *J. Am. Chem. Soc.* **2020**, *142*, 15371–15385.
21 Wu, S.; Yang, H.; Huang, S.; Chen, Q. Relationship between reaction kinetics and chain dynamics of vitrimers based on dioxaborolane metathesis. *Macromolecules* **2020**, *53*, 1180–1190.
22 Röttger, M.; Domenech, T.; van der Weegen, R.; Breuillac, A.; Nicolaÿ, R.; Leibler, L. High-performance vitrimers from commodity thermoplastics through dioxaborolane metathesis. *Science* **2017**, *356*, 62–65.
23 Riehle, N.; Thude, S.; Götz, T.; Kandelbauer, A.; Thanos, S.; Tovar, G. E. M.; Lorenz, G. Influence of PDMS molecular weight on transparency and mechanical properties of soft polysiloxane-urea-elastomers for intraocular lens application. *Eur. Polym. J.* **2018**, *101*, 190–201.
24 Bae, S. C.; Lee, H.; Lin, Z.; Granick, S. Chemical imaging in a surface forces apparatus: Confocal raman spectroscopy of confined poly(dimethylsiloxane). *Langmuir* **2005**, *21*, 5685–5688.
25 Groza, A.; Surmeian, A. Characterization of the oxides present in a polydimethylsiloxane layer obtained by polymerisation of its liquid precursor in Corona discharge. *J. Nanomater.* **2015**, *2015*, 204296.
26 Smith, M. K.; Northrop, B. H. Vibrational properties of boroxine anhydride and boronate ester materials: Model systems for the diagnostic characterization of covalent organic frameworks. *Chem. Mater.* **2014**, *26*, 3781–3795.
27 Ricarte, R. G.; Shanbhag, S. A tutorial review of linear rheology for polymer chemists: Basics and best practices for covalent adaptable networks. *Polym. Chem.* **2024**, *15*, 815–846.
28 Huhtamäki, T.; Tian, X.; Korhonen, J. T.; Ras, R. H. A. Surface-wetting characterization using contact-angle measurements. *Nat. Protoc.* **2018**, *13*, 1521–1538.
29 Wong, W.; Hauer, L.; Naga, A.; Kaltbeitzel, A.; Baumli, P.; Berger, R.; D'Acunzi, M.; Vollmer, D.; Butt, H. Adaptive wetting of polydimethylsiloxane. *Langmuir* **2020**, *36*, 7236–7245.
30 Utrera-Barrios, S.; Yu, L.; Skov, A. L. Revisiting the thermal transitions of polydimethylsiloxane (PDMS) elastomers: Addressing common misconceptions with comprehensive data. *Macromol. Mater. Eng.* **2025**, *310*, 2500075.
31 Fang, H.; Zhang, F.; Zhao, Y.; Gao, X.; Zhou, W.; Qi, G.; Ding, Y.; Winter, H. H. Rheology of smectic liquid crystalline elastomers with dynamic covalent bonds. *Macromolecules* **2023**, *56*, 7808–7817.
32 Chen, Q.; Tudryn, G. J.; Colby, R. H. Ionomer dynamics and the sticky Rouse model. *J. Rheol.* **2013**, *57*, 1441–1462.
33 Krishnakumar, B.; Sanka, R. V. S. P.; Binder, W. H.; Parthasarthy, V.; Rana, S.; Karak, N. Vitrimers: Associative dynamic covalent adaptive networks in thermoset polymers. *Chem. Eng. J.* **2020**, *385*, 123820.
34 Yang, L.; Wang, W.; Wang, Y.; Qu, S.; Yang, M.; Fan, Z.; Bai, R.; Cheng, L.; Yu, W.; Yan, X.; Zhang, Z. Covalent adaptable networks with mobile cross-linking points. *Angew. Chem. Int. Ed.* **2026**, *65*, e19906.
35 Ricarte, R. G.; Shanbhag, S. Unentangled vitrimer melts: Interplay between chain relaxation and cross-link exchange controls linear rheology. *Macromolecules* **2021**, *54*, 3304–3320.
36 Cui, X.; Jiang, N.; Shao, J.; Zhang, H.; Yang, Y.; Tang, P. Linear and nonlinear viscoelasticities of dissociative and associative covalent adaptable networks: Discrepancies and limits. *Macromolecules* **2023**, *56*, 772–784.